NANOSYSTEMS:
PHYSICS, CHEMISTRY, MATHEMATICS

Lukashenko S.Yu., et al. *Nanosystems: Phys. Chem. Math.*, 2025, **16** (4), 441–449.
http://nanojournal.ifmo.ru
DOI 10.17586/2220-8054-2025-16-4-441-449

Original article

Ionic conductivity in nanopipettes: experiment and model

Stanislav Yu. Lukashenko[1,a], Olga M. Gorbenko[1,b], Mikhail L. Felshtyn[1,c], Ivan D. Sapozhnikov[1,d], Demid A. Kirilenko[2,e], Stepan V. Pichakhchi[1,f], Mikhail V. Zhukov[1,g], Alexander O. Golubok[1,h]

[1]Institute for Analytical Instrumentation of the Russian Academy of Sciences, Saint Petersburg, Russian Federation

[2]Ioffe Institute, Saint Petersburg, Russian Federation

[a]lukashenko13@mail.ru, [b]gorolga64@gmail.com, [c]mfelsztyn@yandex.ru, [d]isapojnikov@gmail.com, [e]Demid.Kirilenko@mail.ioffe.ru, [f]pichakhchi.s@yandex.ru, [g]cloudjyk@yandex.ru, [h]aogolubok@mail.ru

Corresponding author: S. Yu. Lukashenko, lukashenko13@mail.ru

ABSTRACT This work investigates ion transport in glass nanopipettes with tip diameters in the range of 80–100 nm, filled with phosphate-buffered saline. A combination of experimental measurements and theoretical modeling is employed. A coupled Poisson-Nernst-Planck-Navier-Stokes model is used to describe the ion transport, incorporating electroosmotic flow, electrophoresis and interionic effects. The theoretical results are in good agreement with experimental current to voltage characteristics. Comparison between modeled and measured data enables estimation of nanopipette geometry with good accuracy. The simulations also reveal characteristic spatial distributions of ionic flow in the aperture area of the nanopipette tip, governed by electroosmosis and the tip shape. These findings provide insights into nanoscale ion transport phenomena relevant for analytical and biological applications.

KEYWORDS Borosilicate nanopipettes, nanopipette geometry, ionic conductivity, electroosmotic flow, ion current rectification.

ACKNOWLEDGEMENTS This work was supported by the Ministry of Science and Higher Education of the Russian Federation (Project No. 075-00444-25-00, dated 26.12.2024) and by the Russian Science Foundation (Project No. 24-79-00169).

FOR CITATION Lukashenko S.Yu., Gorbenko O.M., Felshtyn M.L., Sapozhnikov I.D., Kirilenko D.A., Pichakhchi S.V., Zhukov M.V., Golubok A.O. Ionic conductivity in nanopipettes: experiment and model. *Nanosystems: Phys. Chem. Math.*, 2025, **16** (4), 441–449.

1. Introduction

Glass micropipettes with an aperture diameter of ∼(1-5) μm are among the fundamental tools in electrophysiology. They are also widely employed for intracellular measurements and oocyte fertilization [1, 2], as well as for the study of ion channels in cell membranes [3, 4]. Glass nanopipettes with an aperture diameter of ∼(20–100) nm are extensively used as probes in scanning ion conductance microscopy (SICM) [5] and also find application as solid-state nanopores [6]. Due to their high sensitivity to pH level, electrolyte concentration [7], and the zeta potential of bio- and nanoparticles passing through the aperture [8], NPs are actively utilized as diverse bio- and chemosensors [9, 10], as well as in DNA sequencing [11].

A critical parameter of NPs is the aperture size, which is often determined using expression (1) or its variations [12–15], derived from the orthodox approach that applies Ohm's law to a conical conductor with a linear current-voltage relationship:

$$R_p = \frac{4 \cdot L_b}{k \cdot \pi \cdot d_a \cdot d_b}, \tag{1}$$

where R_p is the resistance of the pipette, k is the conductivity of the solution, d_a and d_b are the aperture diameter and the channel diameter at a distance L_b, respectively (Fig. 1). While Equation (1) generally provides accurate results for systems exhibiting linear I(V) characteristics, its application becomes less reliable when dealing with nanopipettes with aperture diameters below 100 nm and at electrolyte concentrations lower than ∼150 mM.

In these specific cases, the emergence of nonlinear I(V) behavior can lead to discrepancies, as evidenced by comparisons with direct transmission electron microscopy (TEM) measurements. This discrepancy occurs because the overlap of diffuse layer potentials between closely spaced charged nanopipettes inner walls plays a significant role in ionic conductivity. It should be noted that ion current rectification coefficient (*ICR*) in glass NPs, i.e., the ratio of ionic currents at different voltage polarities, demonstrates high sensitivity to a local volume charge density of hydroxide ions, therefore this peculiarity is using for pH sensing [7].

It is important to note several limitations inherent to formula (1). First, the nonlinearity of the I(V) curves in nanopipettes introduces ambiguity in selecting the appropriate segment of the curve for resistance R_p comparison. To address this, we chose resistance values near zero voltage, which also align with the average resistance across the entire curve. Second, determining the specific conductivity of the electrolyte solution poses a challenge. While we initially use a conductivity value of k = 1.9 S/m for PBS solutions [16], which matches our experimental conditions, calculations using this value led to a $\sim$40% discrepancy between the resistance derived by (1) and resistance obtained from experimentally I(V) curve, the same deviation yields nanopipette aperture diameter calculated by (1).

To refine the conductivity value, we performed an additional experiment using a microcapillary with bigger inner diameter 0.69 mm, where the I(V) characteristic remains linear. Corrected PBS conductivity value k =1.55 S/m was calculated from I(V) characteristic using ohmic approach. The aperture diameter calculated by (1) with refined conductivity value reduced the discrepancy with aperture diameter obtained by TEM measurements to $\sim$30%. However, this residual error remains significant for small nonlinearity systems and as our model predicts it grows further when the aperture diameter decreases and the nonlinearity increases. Accordingly, it is necessary to account the interaction of diffusive layers on the nanopipette inner walls.

Negatively charged sites are formed on glass surface when it contacts with aqueous solutions having pH greater than 4 [25]. Also, this negative surface charge forms a double electric and diffusive layers in electrolyte near the glass wall. This leads to specific ion transport near the solid-liquid interface that can significantly differ from that in the solution away from the wall. The unique geometry of the nanopipette, especially at small aperture sizes, results in the formation of depletion and enrichment concentration zones strongly depending on the polarity of the applied voltage. Consequently, the ion currents through the nanoaperture exhibit non-uniform spatial distribution, with ion flux density near the walls of the nanoaperture being significantly higher than along the channel axis. As a result, the I(V) characteristic of the nanopipette tends to be nonlinear under these conditions.

Despite the fact that the properties of NPs are well-studied [14, 15, 17–20], the results of ion current modeling often do not coincide with direct measurements. For example, in works [17, 18], an excessive number of fitting parameters is required to achieve agreement between calculation and experiment. A good qualitative correlation with the experiment is provided by the model [19] that combines the Poisson and Nernst-Planck equations. This model was later extended by adding the Navier-Stokes equation to account for electroosmotic flow through the convective term in the Nernst-Planck equation [20]. This model demonstrates good agreement between theoretical and experimental values of the rectification coefficient; however, the absolute values of the measured ion currents poorly match the modeling results, necessitating the use of fitting parameters such as effective surface charge density, effective diffusion coefficient, or effective aperture diameter of the nanopipette [19, 20].

Given these challenges, direct measurements of crucial geometrical parameters, such as the internal channel angle at the vertex and aperture size of the NP is needed. While the outer angle of the cone, which generally correlates with the internal angle, can be measured using optical or scanning electron microscopy (SEM), the accurate measurement of aperture size requires TEM. However, preparing the sample for TEM typically involves breaking off the nanopipette tip, rendering the nanopipette unusable afterward. Therefore, an important challenge is to determine the aperture size using a non-destructive method based on I(V) characteristics and an adequate model that accounts real nanochannel geometry, surface charge density, electroosmotic flow and diffusion coefficients of the primary charge carriers accounting electrophoretic and relaxation effect caused by interionic interactions and the interaction of an ion with its ionic atmosphere.

Our goal was to identify a model of ion transport in nanopipettes that most accurately reproduces the experimentally measured current–voltage characteristics. Particular attention was given to the influence of the electroosmotic flow on ionic conductivity.

2. Experiment

A batch of 50 NPs was fabricated from borosilicate capillaries (ID = 0.69 mm, L = 15 cm) as blanks. All NPs were produced using puller (MDI PMP 102, USA) and under the same program. The measurements of I(V) dependences were conducted in a 1x PBS solution. Ag/AgCl electrodes were prepared by chlorinating silver wires with a diameter of 300 μm, following the method described in [21]. I(V) characteristics of nanocapillaries were measured using the setup shown in (Fig. 1a), in the same conditions and with the same electrodes. It should be noted that during the measurements, the NPs were held in the PBS solution for 1 hour at zero voltage until the I(V) characteristics stabilized. Currents in the range of $\sim$ (1–10) nA were measured with potentiostatic scheme [22], between the Ag/AgCl electrodes with applied voltage in the range from -1 V to $+1$ V. Ion current rectification coefficients obtained from I(V) characteristics were in the range of (1.0 – 1.5). Fig. 2 shows the distribution of experimentally measured ICR values for nanopipettes fabricated using a single pulling program. For nanopipettes with relatively low (NP No 1), medium (NP No 2), and high conductance (NP No 3) more detailed measurements of tip geometry were carried out after I(V) measurements with TEM. The aperture diameter d_a and the channel diameter d_b at the length L_b of the NPs were measured using TEM JEOL JEM-2100F.

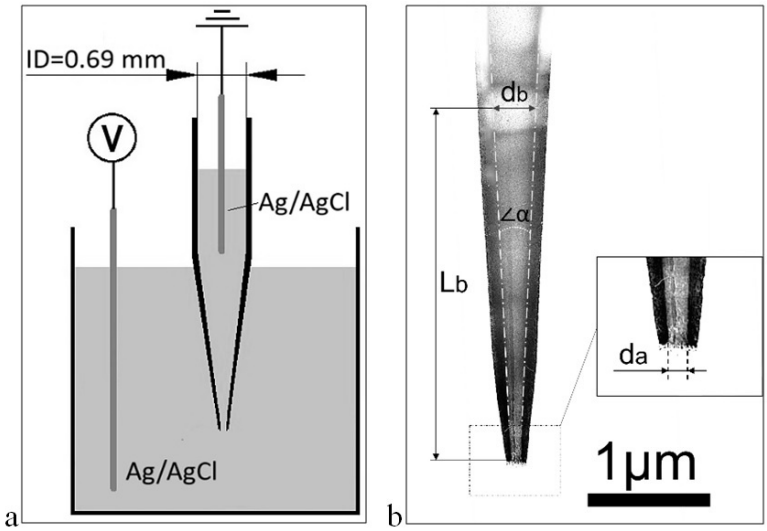

FIG. 1. Experimental setup scheme for measuring I(V) characteristics of nanopipettes (a), and TEM image of the NP-1 tip (b). TEM image obtained after I(V) measurement

The internal angle at the vertex α was determined using the expression:

$$\alpha = 2 \cdot \arctan\left(\frac{\frac{d_b}{2} - \frac{d_a}{2}}{L_b}\right), \tag{2}$$

The obtained geometrical parameters are shown in the Table 1 and were used in subsequent modeling. The experimental I(V) dependence measured for NP No 1 is shown in Fig. 3 by the solid curve. Voltampere characteristics for NPs No 2 and Nov3 were also performed, current values only at ± 1 V are presented in Table 1, as no intermediate data were provided or used in the analysis.

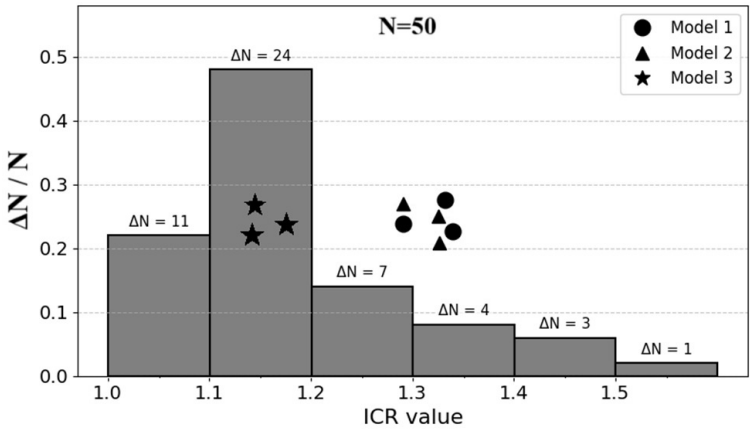

FIG. 2. Histogram of ICR value distribution for nanopipettes made using a same pulling program. Model 3 (star dots) accounts for EOF, while Model 1,2 (circle and triangle dots) does not. The markers on the histogram indicate the calculated ICR values falling into the corresponding ranges for all three nanopipettes according to Model 1, Model 2 and Model 3

3. Model

Given the geometry of the NPs, a two-dimensional axisymmetric problem was solved using "Comsol Multiphysics 6.1". A stationary solution was found for the system of self-consistent equations. The model employed the "Tertiary Current" solver, which solves the Nernst-Planck equation:

$$N_i = -D_i \nabla c_i - z_i F u_i c_i \nabla \Phi + u c_i, \tag{3}$$

where D_i is the diffusion coefficient, u_i is the ion mobility, z_i is the ionic charge, F is the Faraday constant, Φ is the electric potential, u is the velocity vector, c_i is the concentration of ions of a specific sign. The first term accounts for diffusion driven by a concentration gradient, the second term – for migration due to the electric field gradient (electrophoresis), and

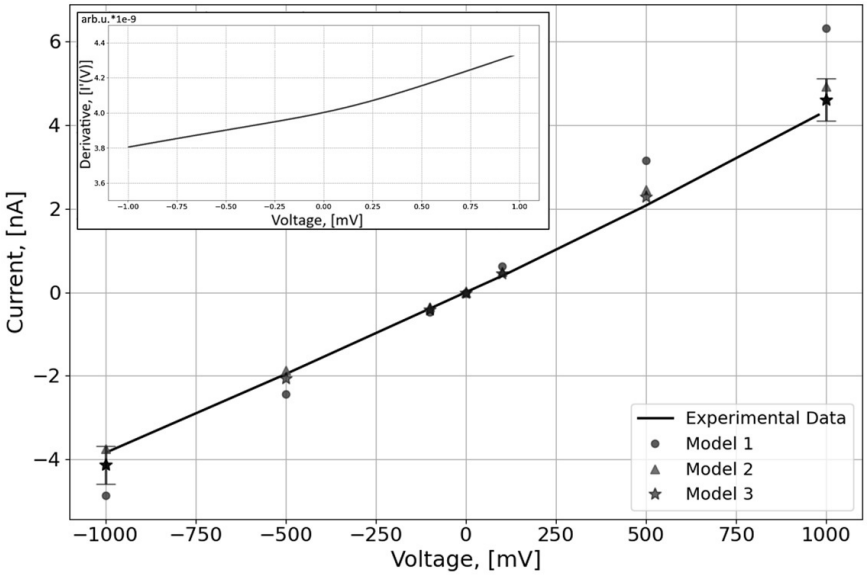

FIG. 3. Experimental and modeled $I(V)$ characteristics of nanopipette (NP-1 in Table 1) with ion current rectification (*ICR* = 1.15). **Models 1**: P-NP simulations neglecting ion-ion interactions; **Models 2–3**: P-NP and P-NP-NS simulations incorporating ion-ion interactions. The inset curve displays the first derivative of the experimental I(V) characteristic, showing its nonlinearity degree. Error bars reflect tolerance in determining macroscopic parameters such as the solution concentration, surface charge density and nanocapillary geometry. Error bars, representing similar tolerance $\sim$10% across all models and displayed only for the best-fitting model (Model 3) at $\pm$1 V to ensure visual clarity

the third term – for electrolyte velocity (convection). The diffusion and migration terms in the Nernst-Planck equation contain diffusion and mobility constants that are assumed to be homogeneous throughout the model domain. Diffusion coefficients for Cl^- and Na^+ were taken from [23], and ion mobility coefficients u_i were calculated using the Nernst-Einstein equation. It is worth noting that the values of the diffusion coefficients are customary for an infinitely diluted solution, however, with an increase in concentration above 0.01 mmol/liter, the Kolrausch law ceases to be performed, and the ionic interaction in the electrolyte cannot be considered insignificantly small [24]. The thermodynamic description of diffusion in solutions taking into account the activity of ions, developed by Lewis, Debye and Onsager [16, 24], makes it possible to take into account the electrophoretic and relaxation effect caused by ionic interactions through a correction for the ion diffusion coefficient:

$$D_i = D_i^0 \left(1 + C_i \cdot \frac{\delta \ln \gamma_i}{\delta C}\right), \tag{4}$$

where D_i^0 is the diffusion coefficient at infinite dilution, C_i is the solution concentration, γ_i is the ion activity coefficient. The ion activity coefficient was calculated in Debye-Hückel approximation.

Additionally, the model assumes a steady-state condition, so:

$$\frac{\partial c}{\partial t} = 0. \tag{5}$$

To construct the double electric layer, the surface charge density q_s was determined using the formula:

$$q_s = -\sqrt{8\varepsilon\varepsilon_0 c_0 kT} \cdot \sin h\left(\frac{ze\phi_0}{2kT}\right), \tag{6}$$

where ε is the dielectric constant of the medium, ε_0 is the vacuum permittivity, k is the Boltzmann constant, T is the temperature, ϕ_0 is the surface potential, z is the valency of the surface bonds, e is the elementary charge.

To calculate the distribution of the electrostatic field in the double electric and diffuse layers, the condition of electroneutrality was disabled. The Poisson equation with volumetric charge was used as the charge conservation model:

$$\nabla^2 \Phi = -\frac{F}{\varepsilon\varepsilon_0} \sum_i z_i c_i, \tag{7}$$

where F is the Faraday constant, z_i is the ionic charge, c_i is the concentration of ions of a specific sign.

The third term in equation (1) accounts for electroosmotic flow (EOF), which arises in the diffuse layer. The EOF velocity was found by solving the Helmholtz-Smoluchowski equation:

$$u_{EOF} = \frac{\xi\, \varepsilon\varepsilon_0}{\mu} \nabla\Phi, \tag{8}$$

where Φ is the electric potential, ξ is the zeta potential of the surface. To determine the surface charge density, we used reference data from a study on the isoelectric point of borosilicate glass [25], which allows us, using known pH (7.4) of the solution in our experiments, to determine the zeta potential for borosilicate glass to be $\sim$30 mV (equivalent surface charge density of -30 mC/m^2).

The EOF velocity in the computational domain was found using the Navier-Stokes equation (Laminar Flow solver):

$$\rho\left(\vec{u}\cdot\nabla\right)\vec{u} = \mu\Delta\vec{u} - \nabla p, \tag{9}$$

where ρ is the electrolyte density, u is the flow velocity, p is the pressure, μ is the kinematic viscosity.

The boundary conditions for equation (9) include a specified uniform velocity at the inlet, slip condition based on the zeta potential on the inner walls of the nanopipette, and constant pressure at the outlet. It is assumed that the laminar flow within the modeled channel is steady, justifying the choice of the Laminar Flow module in Comsol Multiphysics. This assumption is due to the fact that the Reynolds number in nanochannels is essentially less than 1 (while the critical value is usually about 2000), which means the movement of the fluid is stable laminar.

As boundary conditions for the computational domain, the electrode potentials and the constant concentration condition were imposed to simulate the electrolyte volume. These conditions impose restrictions on the size of the computational domain. Initially, the choice of the tip size of the modeled nanopipette is determined by the overall conductivity, which is proportional to the cross-sectional area. Since the nanochannel represents a series of resistors, its overall conductivity is determined by the section with the highest resistance. A computational domain size of 10×10 μm is sufficient because 99% of the voltage applied between the electrode in the beaker and the pipette drops within this region. Additionally, near the boundaries of the computational domain, the concentration should exhibit minimal gradient, simulating the electrolyte cell volume. In the calculations, the mesh for the solver was refined, and the size of the computational domain was increased until the difference in the calculated values of total flux was less than 1%.

It is worth noting that the model data is the calculated ion currents occurring through the nanoaperture of the NP, while an electronic current is measured in the experiment, in the circuit of the electrodes closing Ag/AgCl, which occurs as a result of the reversible electrochemical reaction to both Ag/AgCl electrodes:

$$\mathrm{Ag{+}Cl^-} \rightleftharpoons \mathrm{AgCl{+}e^-} \tag{10}$$

As a result of this reaction, the total mass of silver chloride in the system does not change, it decreases on the cathode and increases on the anode. This electrochemical reaction is considered very fast, the reaction time is about 1 femtosecond, so it is not a limiting factor. The main carriers of the charge in the electrolyte are Na^+ and Cl^-. Ion Cl^- forms an AgCl molecule on the anode and adds one electron to the chain. Sodium ion performs the main work on transferring a positive charge to the volume of the nanochannel, but does not respond with the electrode, this is performed by the Ag^+ ion, which is restored on the cathode to metal silver, while the solution is formed by the Cl^-, which is formed due to the decomposition of the AgCl molecule on the cathode. Thus, the constant concentration of anions and cations in the electrolyte is supported. The charge (or electricity) in electrolytes is transferred to both cations and anions. Therefore, in a state of stationary current, the total flow of cations and anions is equivalent to the flow of electrons involved in the restoration of Ag^+ on the cathode and oxidation of Cl^- at the anode. Since the main carriers of the charge in the narrow region of the capillary are Na^+ and Cl^-, to calculate the total flow of anions and cations in the NP, it is enough to calculate the Na^+ and Cl^- fluxes in this area only.

4. Results and discussions

As can be seen from Fig. 3 that models 2 and 3 provide the best agreement between modelled and experimental absolute currents values; however, due to measurement uncertainty, it is not possible to determine which model is more accurate. However, from Fig. 2, it can be seen that the model accounting for EOF (Model 3) shows better agreement with the experimentally obtained ICR values compared to the model that neglects electroosmotic effects (Model 2).

Consideration of all three terms in Nernst-Planck equation including Onsager equation (4) give the 10% discrepancy between modelled experimental currents values (Table 1). It is worth emphasizing that calculating of ion currents neglecting diffuse coefficient correction (4) in electrolytes with concentrations 0.15 M/l lead to the discrepancy of 30 % with experimental currents (Table 1).

It is evident that this modeling approach can be utilized to evaluate the nanopipette aperture diameter indirectly by knowing the vertex angle of the nanopipette and the experimental I(V) characteristics. Accurate measurement of the NP internal vertex angle is only possible using TEM, which requires breaking off the nanopipette tip for the measurements. However, by analogy with the previous studies within micro- and nanopipettes [27,28], a geometric ratio parameter can be introduced between the internal and outer vertex angles of the nanopipette. Moreover, this coefficient is equal to relation of outer and inner aperture diameters. From the analysis of TEM images of various NPs, we determined this coefficient as $a = \dfrac{\angle\alpha_{inner}}{\angle\alpha_{outer}} = \dfrac{d_{inner}}{d_{outer}}$, which was found to be $a = 0.55 \pm 0.05$. The outer vertex angle can be easily determined, for instance, from SEM image of the NP tip. To conclude, if you could measure the outer angle and the relation between the outer and inner angles or diameters, this model enables to determine the aperture diameter from I(V) measurements with accuracy about 10% that was validated by direct TEM measurements. When the outer diameter and the outer vertex

TABLE 1. Geometric parameters of NP, experimental, and model current values

NP No	Nanopipette geometry			Experiment		Model No 1	Model No 2	Model No 3	Modeled nanopipette geometry	
	d_a, nm	d_b, nm	L_b, nm	U, V	I, nA	I, nA	I, nA	I, nA	d_{a_model}, nm	$\tan(\alpha)$
1	82±2	239±5	4.17±0.1	−1	4.34	5.70	4.61	4.94	82	0.018
				−0.5	2.06	2.81	2.29	2.32		
				−0.1	0.44	0.6	0.49	0.46		
				0.1	−0.42	−0.43	−0.35	−0.41		
				0.5	−2.00	−2.57	−2.09	−2.03		
				1	−3.75	−5.08	−4.13	−3.8		
2	83±2	280±5	4.17±0.1	−1	5.88	7.84	6.58	5.98	83	0.025
				1	−5.10	−6.24	−5.03	−5.29		
3	94±3	331±5	4.17±0.1	−1	8.03	10.37	7.69	7.85	94	0.028
				1	−7.21	−9.37	7.00	−7.10		

angle of the nanopipette are known, but parameter a is unknown or cannot be determined experimentally, the modelling approach presented in this work enables non-destructive determination of the inner aperture diameter by using it as the sole fitting parameter in the comparison between modeled and experimental I–V characteristics.

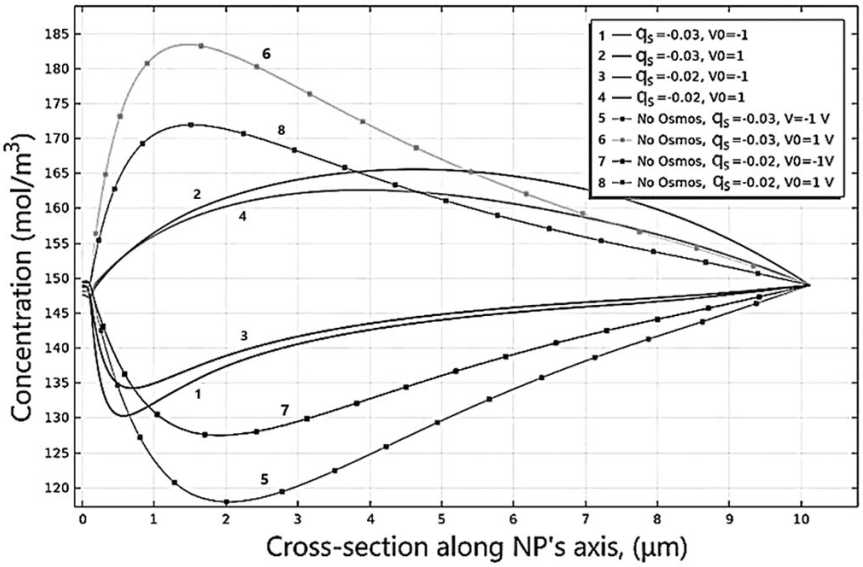

FIG. 4. The effect of electroosmosis on the distribution of equilibrium ion concentration along the nanopipette axis (anion concentration equals cation concentration). The concentration profiles are represented by dotted lines (without electroosmosis) and solid lines (with electroosmosis), respectively (q_s – surface charge density)

Figure 4 shows electroosmosis influence on concentration distribution of cations and anions along the nanopipette axis and surface charge density influence on the EOF under positive and negative polarity. As it was mentioned above, ion conductivity in nanopipettes depends on the voltage polarity applied to the nanopipette. In the case of positive polarity inside the nanopipette, the concentrations increased (profiles 2,4,6,8). In the case of the negative polarity, the concentrations have decreased values (profiles 1,3,5,7). Accounting for the EOF 8% decrease ion concentration and the absolute current values under positive polarity, under negative polarity EOF 8% increase ion concentration and absolute current values, that yields calculation of ICR coefficient with 4% discrepancy in comparison with the experimental value.

Through modeling in [28], it was shown that EOF can also create electrolyte zero-velocity regions near the walls of an NP's aperture. In this work, the authors study NPs with wall thicknesses of 1.5 nm, which is practically difficult to

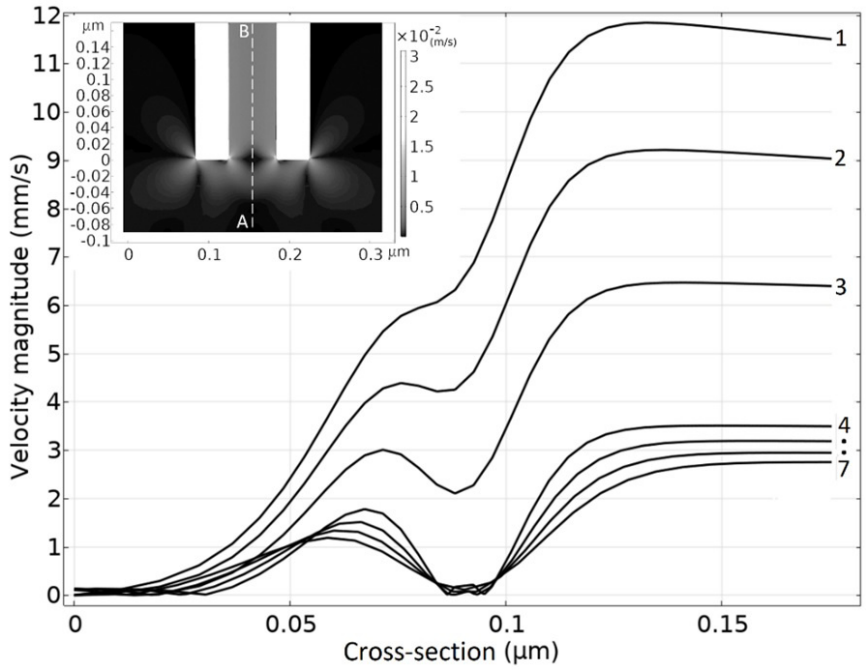

FIG. 5. Convective electrolyte flow velocity profiles along the aperture cross-section (A-B) of the pipette with an r_c = 3 nm and varying vertex geometry of the nanopipette. The picture on the inset shows the velocity distribution in the NP apex area. 1: d_a= 60 nm, $\angle\alpha$= 1.72°; 2: d_a= 60 nm, $\angle\alpha$= 1.26°; 3: d_a= 60 nm, $\angle\alpha$= 0.80°; 4: d_a= 90 nm, $\angle\alpha$= 0.34°; 5: d_a= 80 nm, $\angle\alpha$= 0.34°; 6: d_a= 70 nm, $\angle\alpha$= 0.34°; 7: d_a = 60 nm, $\angle\alpha$= 0.34°

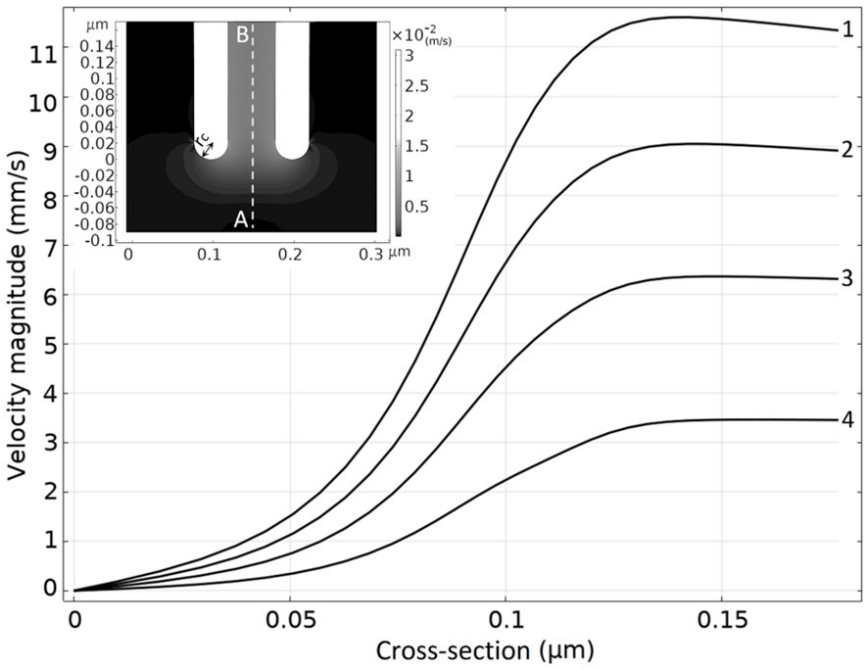

FIG. 6. Convective electrolyte flow velocity profiles along the aperture cross-section (A-B) of the pipette with an r_c = 20 nm and varying vertex geometry of the nanopipette. The picture on the inset shows the velocity distribution in the NP apex area. 1: d_a= 60 nm, $\angle\alpha$= 0.34°; 2: d_a= 60 nm, $\angle\alpha$= 0.80°; 3: d_a= 60 nm, $\angle\alpha$= 1.26°; 4: d_a= 60 nm, $\angle\alpha$= 1.72°

achieve in experiments. We conducted similar calculations for experimentally achievable nanopipette wall thicknesses of 40 nm.

Numerical experiments show that a region with reduced electrolyte velocity can be formed within the nanopipette aperture, but unlike [28], in our case, the zero-velocity region is formed at the center of the aperture rather than near the walls. It was found that this feature depends on the curvature radius of the aperture edges (r_c) and the vertex angle of the nanopipette. In NPs with $r_c = 3$ nm, the vertex angle less than 0.34 degree and the aperture radii of (60–90) nm, an electrolyte zero-velocity area appears in the nanopipette aperture (Fig. 5), whereas with $r_c = 20$ nm, such a region is absent (Fig. 6).

This feature arises in NPs with $r_c = 3$ nm and with a surface charge density on the borosilicate nanopipette walls of -30 mC/m^2 (at pH = 7.4 in 1x PBS). The Debye length at the electrolyte concentrations 150 mM/L is about 1 nm, and further reduction of the curvature radius lacks physical meaning. Additionally, it was found that the aperture edge curvature radius in the range (3–20) nm does not significantly affect the absolute values of the total ion fluxes and the currents (less than 1%).

5. Conclusions

Thus, the model, which takes into account interionic interactions in the solution and the electroosmotic flow through convective term in the Nernst-Planck equation, demonstrates good agreement between the experimental and calculated ICR values with an accuracy of 4%. Moreover, the model enables non-destructive estimation of the inner aperture diameter from the known outer diameter and the outer vertex angle of the nanopipette by fitting experimental and theoretical I(V) curves.

In addition, the calculation shows that for some NP's wall topologies in the velocity field of the electrolyte in the NP's aperture the zero-velocity region appeared. Considering that NP can act as a molecular translocation nanopore sensor, this may be useful to improve a molecular detection sensitivity.

References

[1] Yaul, M.; Bhatti, R.; Lawrence, S. Evaluating the process of polishing borosilicate glass capillaries used for fabrication of in-vitro fertilization(iVF) micro-pipettes. *Biomed Microdevices.* 2008, **10**, 123–128.

[2] Brown K.T. Flaming D.G. *Advanced micropipette techniques for cell physiology*. Wiley, San Francisco, 1995.

[3] Sakmann B., Neher E. *Single-channel recording*. Plenum Press, New York, 1983.

[4] Neher E., Sakmann B. Single-channel currents recorded from membrane of denervated frog muscle-fibers. *Nature*, 1976, **260**, P. 799–802.

[5] Page A., Perry D., Unwin P.R. Multifunctional scanning ion conductance microscopy. *Proc. R. Soc. A.*, 2017, **473**, P. 20160889.

[6] Stuber A., Schlotter T., Hengsteler J., Nakatsuka N. *Solid-State Nanopores for Biomolecular Analysis and Detection.* In: Lisdat F., Plumeré, N. (eds) Trends in Biosensing Research. Advances in Biochemical Engineering/Biotechnology, Springer, Cham, 2023, **1**, P. 187.

[7] Wang X.F., Duan Y.F., Zhu Y.Q., Liu Z.J., Wu Y.C., Liu T.H., Zhang L., Wei J.F., Liu G.C. An insulin-modified pH-responsive nanopipette based on ion current rectification. *Sensors*, 2024, **24**(13), P. 4264.

[8] Wang Y., Kececi K., Mirkin M.V., Mani V., Sardesai N., Rusling J.F. Resistive-pulse measurements with nanopipettes: detection of Au nanoparticles and nanoparticle-bound anti-peanut IgY. *Chem Sci.*, 2013, **4**(2), P. 655–663.

[9] Kececi K., Dinler A., Kaya D. Review – Nanopipette applications as sensors, electrodes, and probes: A study on recent developments. *J. Electrochem. Soc.*, 2022, **169**(2), P. 027502.

[10] Xu C., Yang D., Wang Y., Liu R., Wang F., Tian Z., Hu K. Micro/nanoelectrode-based electrochemical methodology for single cell and organelle analysis. *Nano Research*, 2024, **17**(1), P. 196–206.

[11] Sze J.Y.Y., Ivanov A.P., Cass A.E.G. et al. Single molecule multiplexed nanopore protein screening in human serum using aptamer modified DNA carriers. *Nat. Commun.*, 2017, **8**, P. 1552.

[12] Nitz H., Kamp J., Fuchs H. A combined scanning ion-conductance and shear-force microscope. *Probe Microsc.*, 1998, **7**(1), P. 187–200.

[13] Terejanszky P., Makra I., Furjes P., Gyurcsanyi R.E. Calibration-less sizing and quantitation of polymeric nanoparticles and viruses with quartz nanopipettes *Anal. Chem.*, 2014, **86**, P. 4688–4697.

[14] Constantin D., Siwy Z. Poisson-Nernst-Planck model of ion current rectification through a nanofluidic diode. *Phys. Rev. E.*, 2007, **76**, P. 041202.

[15] Chaparro C.V., Herrera L.V., Meléndez A.M., Miranda D.A. Considerations on electrical impedance measurements of electrolyte solutions in a four-electrode cell. *J. Phys. Conf. Series*, 2016, **687**, P. 012101.

[16] Perry D., Momotenko D., Lazenby R.A., Kang M., Unwin P.R. Characterization of nanopipettes. *Anal. Chem.*, 2016, **88**, P. 5523–5530.

[17] Woermann D. Analysis of non-ohmic electrical current–voltage characteristic of membranes carrying a single track-etched conical pore. *Nucl. Instrum. Methods Phys. Res., Sect. B*, 2002, **194**, P. 458–462.

[18] Woermann D. Electrochemical transport properties of a cone-shaped nanopore: high and low electrical conductivity states depending on the sign of an applied electrical potential difference. *Phys. Chem. Chem. Phys.*, 2003, **5**, P. 1853.

[19] Cervera J., Schiedt B., Ramirez P.A Poisson/Nernst-Planck model for ionic transport through synthetic conical nanopores. *Europhys. Lett.*, 2005, **71**, P. 35.

[20] Apel P., Korchev Y.E., Siwy Z., Spohr R., Yoshida M. Diode-like single-ion track membrane prepared by electro-stopping. *Nucl. Instrum. Methods Phys. Res., Sect. B*, 2001, **184**, P. 337.

[21] Tao D., Jiang L. & Jin M. A Method of preparation of Ag/AgCl chloride selective electrode. *J. Wuhan Univ. Technol.-Mat. Sci. Edit.*, 2018, **33**, P. 767–771.

[22] Lukashenko S.Y. et al. Behavioral features of the approach curve of a scanning ion-conductance microscope. *J. Surf. Investig*, 2023, **17**, P. 585–591.

[23] Laurance N. Self-diffusion of the chlorine ion in sodium chloride. *Phys. Rev.*, 1960, **120**, P. 57–62.

[24] Girault H.H. *Analytical and Physical Electrochemistry*. New York, EPFL Press, 2004.

[25] Amadu M., Miadonye A. Determination of the point of zero charge PH of borosilicate glass surface using capillary imbibition method. *Int. J. Chem.*, 2017, **9**, P. 67–84.

[26] Brown K.T., Flaming D.G. *Advanced micropipette techniques for cell physiology*, John Wiley & Sons, New York, 1986.
[27] Rheinlaender J., Schäffer T.E. An accurate model for the ion current-distance behavior in scanning ion conductance microscopy allows for calibration of pipet tip geometry and tip-sample distance. *Anal. Chem.*, 2017, **89**, P. 11875–11880.
[28] Rabinowitz J., Edwards M.A., Whittier E., Jayant K., Shepard K.L. Nanoscale fluid vortices and nonlinear electroosmotic flow drive Ion current rectification in the presence of concentration gradients. *J. Phys. Chem. A* , 2019, **123**(38), P. 8285–8293.

Submitted 14 June 2025; revised 26 June 2025; accepted 27 June 2025

Information about the authors:

Stanislav Yu. Lukashenko – Institute for Analytical Instrumentation of the Russian Academy of Sciences, Saint Petersburg, Russian Federation; ORCID 0000-0002-5356-1261; lukashenko13@mail.ru

Olga M. Gorbenko – Institute for Analytical Instrumentation of the Russian Academy of Sciences, Saint Petersburg, Russian Federation; ORCID 0000-0002-7054-6602; gorolga64@gmail.com

Mikhail L. Felshtyn – Institute for Analytical Instrumentation of the Russian Academy of Sciences, Saint Petersburg, Russian Federation; ORCID 0000-0001-8677-061X; mfelsztyn@yandex.ru

Ivan D. Sapozhnikov – Institute for Analytical Instrumentation of the Russian Academy of Sciences, Saint Petersburg, Russian Federation; ORCID 0000-0003-2575-5015; isapojnikov@gmail.com

Demid A. Kirilenko – Ioffe Institute, Saint Petersburg, Russian Federation; ORCID 0000-0002-1571-209X; Demid.Kirilenko@mail.ioffe.ru

Stepan V. Pichakhchi – Institute for Analytical Instrumentation of the Russian Academy of Sciences, Saint Petersburg, Russian Federation; ORCID 0000-0002-8578-5200; pichakhchi.s@yandex.ru

Mikhail V. Zhukov – Institute for Analytical Instrumentation of the Russian Academy of Sciences, Saint Petersburg, Russian Federation; ORCID 0000-0003-3361-6947; cloudjyk@yandex.ru

Alexander O. Golubok – Institute for Analytical Instrumentation of the Russian Academy of Sciences, Saint Petersburg, Russian Federation; ORCID 0000-0001-9970-9172; aogolubok@mail.ru

Conflict of interest: the authors declare no conflict of interest.